Crystal structure of zinc-α2-glycoprotein in complex with a fatty acid reveals multiple different modes of protein-lipid binding

Andy M. Lau[1†], Henna Zahid[1], Jayesh Gor[1], Stephen J. Perkins[1], Alun R. Coker[2], and Lindsay C. McDermott[3]*

[1] Department of Structural and Molecular Biology, University College London, Darwin Building, Gower Street, London WC1E 6BT, U.K.

[2] University College London, Division of Medicine, The Rayne Building, 5 University Street, London, WC1E 6JF, U.K.

[3] School of Life Sciences, University of Bedfordshire, Park Square, Luton LU1 3JU, U.K.

[†]Present address: Department of Chemistry, King's College London, 7 Trinity Street, London SE1 1DB, UK

‡ Author to whom correspondence and requests for reprints should be addressed (School of Life Sciences, University of Bedfordshire, Park Square, Luton LU1 3JU, U.K, Tel: +44 (0)1582 489 644; Fax: +44 (0)1582 489 212; e-mail: lindsay.mcdermott@beds.ac.uk)

Running title: Crystal structure of zinc-α2-glycoprotein and DAUDA

Key words: Analytical ultracentrifugation; DAUDA; fluorescence; obesity; x-ray crystallography

Abbreviations: AUC, analytical ultracentrifugation; DAUDA, 11-(dansylamino)undecanoic acid; DHA, docosahexaenoic acid; FABP1, human intracellular liver fatty acid binding protein; FABP2, intracellular intestinal fatty acid binding protein; HSA, human serum albumin; MHC, major histocompatibility complex; PEG, polyethylene glycol; ZAG, zinc-α2-glycoprotein.

Abstract (250 words) (Background, aims, results, conclusions)

Human zinc-α2-glycoprotein (ZAG) is a 42 kDa adipokine which regulates body fat mass and is associated with cachexia and obesity. ZAG belongs to the major histocompatibility complex class I protein family and binds long chain polyunsaturated fatty acids in its groove formed from the α1 and α2 domains. To identify the molecular basis of its lipid-binding function, we determined the first crystal structure at 2.49Å resolution for fatty acid-bound ZAG, where the ligand was the fluorescent 11-(dansylamino)undecanoic acid (DAUDA). The 192 kDa crystallographic asymmetric unit contained six ZAG and eight fatty acid molecules in unique conformations. Six fatty acid molecules were localised to the ZAG grooves, where its tails were bound in two distinct conformations. The carboxylate groups of three fatty acids projected out of the groove, while the fourth was hydrogen bonded with R73 inside the groove. Other ligand-residue contacts were primarily hydrophobic. A new fatty acid site was revealed for two further DAUDA molecules at the ZAG α3 domains. Following conformational changes from unbound ZAG, the α3 domains formed tetrameric β-barrel structures lined by fatty acid molecules that doubled the binding capacity of ZAG. Analytical ultracentrifugation revealed that ZAG in solution was a monomer in the absence of DAUDA, but formed small amounts of tetramers with DAUDA. By showing that ZAG binds fatty acids in different locations, we demonstrate an augmented mechanism for fatty acid binding in ZAG that is distinct from other known fatty acid binding proteins, and may be relevant to cachexia.

Summary statement (40 words): The first crystal structure for fatty acid-bound zinc-α2-glycoprotein revealed fatty acid binding in its main groove formed by its α1 and α2 domains, and a further fatty acid binding site within a tetramer of α3 domains.

INTRODUCTION

Zinc-α2-glycoprotein (ZAG) is a 42 kDa adipokine first purified from human plasma by precipitation with zinc acetate [1]. ZAG has since been located in secretory epithelial cells and body fluids [2, 3]. ZAG is identical to a lipid mobilizing factor purified from the urine of patients with cancer cachexia and promotes lipolysis and browning of white adipose tissue [4, 5]. Its expression in adipocytes is inversely related to body fat mass such that ZAG mRNA and protein expression are decreased in adipocytes from obese mice and patients [6, 7]. ZAG-deficient mice increased body weight when fed a lipid rich diet [8] while the over expression of ZAG in ob/ob mice reduced body weight and white adipose tissue mass [9]. ZAG stimulates lipolysis through activation of the β3-adrenergic G-protein-coupled receptor in mice [10]. The dysregulation of ZAG in inflammatory disease [11-14] and cancer [15-18], including obesity and cachexia, continues to be re-emphasised together with its role in lipid metabolism.

ZAG is a member of the major histocompatibility complex (MHC) class I protein family with α1, α2 and α3 domains. It is distinct from other members of this protein family in that the classic α1-α2 α-helical groove binds small hydrophobic molecules [19] rather than peptides, and the α3 domain associates with prolactin inducible protein rather than with β2 microglobulin [20]. The original crystal structure of human plasma ZAG contained unresolved electron density in the α1-α2 groove at the same location where peptides classically bind to class I MHC proteins [21]. This density was later determined to be polyethylene glycol (PEG), a precipitant used for ZAG crystallisation [22]. Eleven conserved residues surrounded PEG in this crystal structure (F77, I76, Y14, R73, F101, Y161, Y154, Y117, W148, W134 and W115). These residues were hydrophobic with the exception of the positively charged R73. In other fatty acid binding proteins such as intracellular fatty acid binding proteins, an arginine residue anchors the negatively charged carboxyl group of fatty acids within otherwise hydrophobic binding sites [23]. Fluorescence displacement assays using 11-(dansylamino)undecanoic acid (DAUDA) revealed that the PEG and DAUDA binding sites were coincident and that ZAG preferentially binds polyunsaturated fatty acids [19, 22]. DAUDA is a saturated C_{11} fatty acid fluorescent probe with a dansyl group attached to its ω-methyl terminus (Figure 1C). DAUDA has been widely used in the characterization of fatty acid binding proteins from nematodes [24-26], schistosomes [27], human intracellular fatty acid binding proteins [28] and human serum albumin (HSA) [29, 30]. The location of the ZAG PEG/DAUDA binding site was confirmed by site-directed mutagenesis [31] which showed that Y14, F77, I76, Y154, Y161 and R73 were crucial for DAUDA binding. Recombinant *Escherichia coli* ZAG contained one tight and fifteen loose zinc binding sites [32], the latter thought to be responsible for the precipitation of ZAG from human plasma during its purification [1]. ZAG also bound the boron dipyrromethene fatty acid C_{16} (BODIPY), and zinc caused ZAG to form oligomers to reduce BODIPY binding but not DAUDA binding [33]. These data indicated the presence of multiple fatty acid binding sites in the ZAG groove, similar to those seen in the structurally related CD1 immune proteins that bind bacterial lipids [34].

The identity of ZAG's physiological ligand remains unknown, yet this information is crucial to understanding the molecular basis of how ZAG regulates body fat mass. To clarify the mechanism of fatty acid binding to ZAG and how this relates to disease, we solved the crystal structure of ZAG in complex with the widely-used fatty acid derivative DAUDA, to 2.49Å resolution. To our knowledge, this represents the first crystal structure of a ZAG-fatty acid complex. This structure revealed two unique modes of lipid binding, one in a flexible groove between the ZAG α1-α2 domains, and the other inside a β-barrel formed by the self-

association of four α3 domains. ZAG thus binds at least twice the expected amount of fatty acid than expected. The extent to which monomeric and tetrameric ZAG-DAUDA complexes were present in solution was examined using analytical ultracentrifugation (AUC).

EXPERIMENTAL

ZAG protein purification

A pET23a clone containing human ZAG was expressed in *E. coli* BL21 (DE3) pLysE cells to produce protein inclusion bodies when induced with isopropyl β-D-1-thiogalactopyranoside. ZAG was purified from these inclusion bodies by refolding using 6 M guanidine hydrochloride and a hyper-dilution method as previously described [32]. Refolded ZAG was purified using a GE Superdex 75 size-exclusion chromatography column equilibrated with phosphate buffered saline (PBS; 2.7 mM KCl, 1.5 mM KH_2PO_4, 137 mM NaCl, 8 mM Na_2HPO_4) at a flow rate of 2 ml/min using an AKTA Pure and Unicorn software. Fractions corresponding to the ZAG elution peak were collected. The Superdex 75 column was calibrated using gel filtration standards (Bio-Rad, Hertfordshire, UK). The elution volumes (V_e) of each gel filtration standard and ZAG were used to calculate K_{av} values where $K_{av} = V_e - V_0 / V_c - V_0$ with a column volume (V_c) of 120 ml and a void volume (V_0) of 44.9 ml. A graph of K_{av} against $\log_{10}$MW of the standard proteins was used to estimate the size of ZAG using its K_{av} value. The purity of *E. coli* ZAG was confirmed by 4-20% non-denaturing gradient SDS PAGE. Purified ZAG was stored at -20°C before use in experiments. Prior to setting up crystallisations, ZAG was subjected to Superdex 75 size exclusion chromatography to remove any potential aggregates formed by freezing. Protein concentrations were determined using a Genesys 10uv scanning spectrophotometer (Thermo Electron Corporation), with a theoretical ε_{280} value of 71,071 cm^{-1} M^{-1} and a molecular mass of 32 276 Da (calculated from the amino acid composition; [35]. Samples were dialysed against Hepes (4-(2-hydroxylethyl)-1-piperazineethanesulfonic acid) - NaOH buffer pH ~7 when required.

Fluorescence spectroscopy

Fluorescence measurements were recorded at 22°C with a Perkin Elmer LS50B Luminescence Spectrometer using 2 ml samples in a quartz cuvette of path length 1 cm. The fluorescent fatty acid probe DAUDA (Thermo Fisher Scientific Technologies, Basingstoke, UK) was stored as a stock solution of ~2 mg/ml in methanol in the dark at -20°C before being diluted into ethanol and then PBS or Hepes buffer. DAUDA concentrations were determined spectrophotometrically using ε_{335} = 4800 M^{-1} cm^{-1} in methanol as specified by the manufacturer. The fluorescence emission intensity of DAUDA was examined in PBS and Hepes buffer and upon sequential additions of ZAG (PBS and Hepes) and defatted human serum albumin (PBS; λ_{ex} = 345 nm). Fatty acid-free albumin (Sigma. Dorset, UK) was reconstituted in PBS buffer prior to use in DAUDA titrations. The reconstituted albumin protein concentration was confirmed spectrophotometrically using ε_{335} = 38,553 M^{-1} cm^{-1}. Fluorescence spectra were corrected for the effects of dilution. Solvent Raman scattering was corrected by subtracting the buffer-only spectrum from each individual spectra. The resulting titration curves were fitted using standard non-linear regression techniques to a single non-competitive binding model to generate dissociation constant K_d values [32]. Results of competition experiments in which docosahexaenoic acid (DHA) was progressively added to a DAUDA:ZAG pre-formed complex were analysed using previously-reported expressions [36] to determine the apparent K_i value for DHA binding to ZAG. A stock solution of 1 mg / ml DHA in ethanol was diluted in PBS, and increasing concentrations of DHA were added to a mixture containing 0.9 μM DAUDA and 0.87 μM ZAG.

Crystallization of ZAG complexes

Crystallization screens were performed with the hanging-drop vapour-diffusion method using 24-well Linbro style plates (Molecular Dimensions Limited, Suffolk, UK). Individual crystals were cryoprotected in paratone:paraffin oil (50:50), and mounted using 0.1-0.2 mm CryoMount LithoLoops (Molecular Dimensions Limited, Suffolk, UK). Crystals were cooled to 100°K using a Cryostream (Oxford Cryosystems, Long Hanborough, UK) and screened for diffraction quality on an X8 Prospector (Bruker, Billerica, Massachusetts, USA) and then stored in 16-sample uni-pucks at 77°K in a cryogenic dewar prior to data collection. The strongest-diffracting crystals of ZAG-C_{11} DAUDA were grown using 2 µl ZAG:DAUDA (1: 1.5) hanging drops. This was prepared from a 1 µl solution containing 310 µM ZAG and 460 µM DAUDA in 16 mM Hepes, pH 7, 0.016% NaN_3, 20% methanol which was mixed with 1 µl of 1.3 M ammonium sulfate, 100 mM Hepes, pH 7.5. The buffer reservoir contained 1.3 M ammonium sulfate, 20 mM Hepes, pH 7.59.

Crystallography data collection and processing

X-ray diffraction data from ZAG-DAUDA crystals were collected at the Diamond Light Source (Didcot, UK) operating at 3 GeV in 900 electron bunch filling mode. Data were collected from the I02 and I03 beamlines at wavelengths of 0.9763 Å and 0.9795 Å respectively, and processed using Xia2 software. The strongest diffracting ZAG:DAUDA crystal was indexed in the I4 space group (Table 1). The quality of the MTZ reflection data were assessed using Phenix.xtriage [37] in which Matthew's coefficient (Vm), the number of molecules in the asymmetric unit (Z), the twin fraction, twin law and twinning type were determined (Table 1). For molecular replacement, data from crystals in the I4 space group were detwinned using Detwin [38, 39] (CCP4), applying the relevant twin fraction and twin law (Table 1). The twinned data was used for refinement.

Maximum-likelihood molecular replacement was performed using phaser-MR [37] (Phenix) using the α1-α2 domain of human ZAG as the search model (PDB ID: 1T7V, accessed from the PDB REDO database). The α3 domain was manually built using COOT followed by refinement cycles with Phenix refine and a twin law of –h, k, -l. The Grade web server was used to generate restraint files for DAUDA (Grade, version 1.2.9, http://www.globalphasing.com) and DAUDA molecules were fitted into positive electron density from composite omit maps generated using Phenix-refine. Final refinement was performed with REFMAC 5.8 [40] with automatic twin refinement. The ZAG-DAUDA contacts were identified using LigPlot Plus software [41].

Analytical ultracentrifugation (AUC)

AUC sedimentation velocity experiments were performed using multi-wavelength Optima and Proteome XL-I Beckman-Coulter instruments equipped with an An50Ti rotor, using cells with two-sector aluminium centrepieces at rotor speeds of 50,000 rpm at 20°C. Experiments on the Optima were performed with 6.2 µM ZAG in 20 mM Hepes buffer, pH 7.6 and PBS pH 7.4. Both samples were titrated with two C_{11} DAUDA at concentrations of 6.2 µM and 62 µM. SEDFIT software (version 15.1) was used to analyse the absorbance data recorded at 280 nm and 335 nm. The Lamm equation was directly fitted to every fifth boundary scan in a total of 112 scans in order to obtain the size distribution analysis *c(s)* that provided the sedimentation coefficient corrected to 20°C in water ($s_{20,w}$) and molecular mass. The *c(s)* analyses were based on a fixed resolution of 200, minimum and maximum sedimentation coefficients (S_{min} and S_{max}) of 0.5 S and 15 S respectively, a frictional ratio of 1.2, a meniscus position of 6.2 cm, a cell bottom of 7.0 cm, a confidence level (F-ratio) of 0.95, a partial specific volume of 0.730 ml/g, buffer densities of 1.00543 g/ml and 0.99978 g/ml, and buffer viscosities of 0.01002 cp and 0.01064 cp for PBS and Hepes respectively; all values being

calculated using SEDNTERP [42]. The baseline, meniscus and bottom of the cell were floated during fitting. The amounts of ZAG monomer and dimers were quantitated using the integration function in the *c(s)* analyses.

Further sedimentation velocity experiments on the XL-I were carried out using high ZAG concentrations (155 μM ZAG) and upon addition of DAUDA in ethanol (1:1.6) in 20 mM Hepes, 137mM NaCl, pH 7 and tracked using interference optics. The buffer densities of 1.00575 g / cm^3 (buffer) or 0.99106 g / cm^3 (buffer with 9% ethanol) were determined using an Anton Paar DMA 5000 density meter. The viscosities of 0.010322 cP (buffer) or 0.013988 cP (buffer with 9% ethanol) were determined using an Anton Paar Microviscometer AMVn. Interference data were analysed using SEDFIT software as described above except that every second boundary scan of a total of 80 (ZAG) or 100 (ZAG:DAUDA) scans were used.

RESULTS

ZAG purification and DAUDA binding affinity.

In order to obtain the three dimensional structure of the ZAG:DAUDA complex, we first purified recombinant *E. coli* ZAG from inclusion bodies. As expected, refolded ZAG produced a single peak with an elution volume of approximately 88 ml on size exclusion chromatography corresponding to an estimated mass of 33.8 kDa (Figure 1A). Refolded and purified ZAG yielded a single band of approximately 32 kDa on 4–20% non-reducing SDS-PAGE (Figure 1B). To confirm the affinity of ZAG for DAUDA, and compare this with that of HSA, DAUDA was titrated with increasing concentrations of ZAG in PBS and Hepes buffers, and likewise HSA in PBS buffer alone (Figure 2). The comparison of DAUDA binding to ZAG and HSA clarified the physiological function of ZAG. DAUDA has a low fluorescence emission intensity which becomes blue-shifted upon sequential additions of ZAG and HSA (Figures 2A-C). The spectral shifts are indicative of DAUDA binding at a hydrophobic binding site in both proteins and are accompanied by an increase in fluorescence emission intensity which was substantially greater for HSA than ZAG (Figures 2A-C). The DAUDA fluorescence emission wavelength shifted from 540 nm to 515 nm upon addition of ZAG (in both PBS and Hepes buffers) and to 490 nm upon addition of HSA. Notably, the shift upon addition of ZAG was less than that observed upon the addition of HSA. This suggested that the DAUDA binding site within ZAG was more solvent exposed than that of HSA. Assuming 1:1 binding in the fits, titrations of ZAG and HSA with DAUDA gave dissociation constants K_d of 0.11 ± 0.02 μM for the tightest of the DAUDA binding sites in HSA, 0.43 ± 0.15 μM for ZAG in PBS and 0.51 ± 0.04 μM for ZAG in 20 mM Hepes pH 7.45 (Figure 2D). Our measurements indicated that ZAG bound DAUDA to a similar degree in the crystallisation (Hepes) and physiological buffers (PBS), and that HSA bound DAUDA more tightly than ZAG, making it likely that a physiological ligand of ZAG is a fatty acid.

To show that the fluorescent dansyl group of DAUDA did not drive the ZAG:DAUDA interaction, a fluorescence competition experiment was performed. Consecutive additions of the untagged DHA to a pre-formed ZAG:DAUDA complex caused a reduction in the fluorescence emission intensity but no red shift in the fluorescence emission wavelength (Figure 2E). Notably the original DAUDA signal was not recovered despite the addition of excess ~ 65 μM DHA to a ZAG:DAUDA complex with 0.9 μM DAUDA. Assuming 1:1 ZAG:DAUDA binding and 1:1 ZAG:DHA binding, an apparent K_i of 10 μM was measured for the ZAG:DHA interaction (Figure 2F).

Crystallisation of the ZAG:DAUDA complex.

Previous attempts to investigate the molecular basis of DAUDA binding to ZAG used pre-formed ZAG crystals grown in the absence of PEG and soaked in 20 μM DAUDA. These crystals diffracted to 3 Å resolution and the DAUDA electron density could not be resolved [22]. Here, we followed an alternative route, in which a 1:1.5 ratio of ZAG to DAUDA in solution was crystallised in the absence of PEG using ammonium sulfate. Crystals of the ZAG-DAUDA complex were obtained in the tetragonal *I4* space group with unit cell parameters $a = b = 167.01$ Å and $c = 204.95$ Å (Figure 1C, Table 1[43]). While the crystal and resulting dataset were twinned, the crystal structure was solved and refined to 2.49 Å resolution through molecular replacement (Methods). The electron density map revealed well-resolved features that corresponded to DAUDA ligand molecules.

The crystallographic ZAG:DAUDA asymmetric unit contained six ZAG molecules positioned with their grooves opposing one another (Figure 3A). Intriguingly, the α3 domains of each ZAG:DAUDA complex moved by an angle of 25˚ towards the α2 helix of the ZAG groove when compared to the α3 domains in previously published apo-ZAG structures. This α3 movement enabled the formation of three 16-stranded β-barrel α3 tetramers within the crystal. In each tetramer, the classic DEBA β-sheets of the four immunoglobulin folds of the α3 domains were hydrogen-bonded to each other through the pairings of the outermost β-strands D and A from adjacent β-sheets. Two of the tetramers were assembled from four chain A α3 domains (AAAA) and four chain B α3 domains (BBBB; Figure 3B). Both these tetramers were positioned on symmetry axes. The final tetramer was formed from the α3 domains of chains CDEF and was not formed around a symmetry axis.

The refined crystal structure revealed six clear areas of positive electron density in five ZAG molecules at or in the α1-α2 groove in the ZAG:DAUDA asymmetric unit. Even though the ZAG structure was solved to a higher resolution than previously, and this was extensively refined, this positive density was broken for regions of the fatty acid tails. There was a large positive peak consistent with the sulphur of the DAUDA sulphonyl group (Figure 1B). The remainder of the DAUDA molecule fitted well to the remaining areas of electron density (Figures 4A,B,C first column). Areas of positive electron density in the equivalent region of chain A were insufficient to support modelling of a DAUDA molecule, but were suggestive of DAUDA binding at low occupancy.

Two distinct DAUDA binding sites were revealed in sufficient detail for a molecular interpretation. Six of eight DAUDA molecules were located close to or bound within the binding grooves of the α1-α2 domains in five ZAG chains B, C, D, E and F, leaving the single chain A empty. Four of these DAUDA were located in each of the grooves of four ZAG chains B, D, E and F while the remaining two DAUDA tethered the opposing α1-α2 grooves of ZAG chains B and C to form a potential ZAG dimer (Figure 3A and Figures 6A-C). Surprisingly a further two DAUDA molecules were bound to each of the α3 domains of ZAG chains A and B (Figure 3B and Figures 6A, B). These DAUDA molecules were located at the face of the four-stranded β-sheets of each α3 domain. This positioning meant that four DAUDA molecules were located inside each of the two chain A and chain B β-barrel ZAG tetramers (Figure 3B).

Overall eight DAUDA molecules were contained within the ZAG:DAUDA asymmetric unit (Figure 3A), this being in good agreement with the 1:1.5 ZAG:DAUDA molar ratio used in co-crystallization. The ZAG:DAUDA asymmetric unit contained four groove-bound ZAG:DAUDA complexes (chains B, D, E and F), two groove-tethered DAUDA complexes (chains B and C), one empty ZAG α1-α2 binding groove (chain A), and two α3-bound

DAUDA molecules (chains A and B). This stoichiometry was in keeping with the ITC-generated K_d value of 1.5 μM for ZAG:DAUDA binding [19] and our values of 0.43 μM and 0.51 μM above (Figure 2). These K_d values were based on the assumption of one DAUDA binding site per ZAG. If multiple DAUDA binding sites exist on ZAG, as suggested by our crystal structure, ITC experiments would not have resolved these, and our K_d values will represent the tightest DAUDA binding site on ZAG. It is likely that DAUDA binds more strongly to the α1 - α2 groove than to the ZAG α3 domain.

Movement of the ZAG α1-α2 groove.

In order to examine each DAUDA groove binding site in more detail, pairs of ZAG chains E and F, B and C, and A and D were superimposed upon one another and pairwise root mean squared deviation (RMSD) comparisons were performed (Figures 4A-C, second column). An RSMD of 0.921 Å was observed for all ZAG atoms of chain B compared with chain C, suggesting a structural movement had occurred in one of these two ZAG chains. Chains E and F were similar, as were chains A and D, with lower average RSMD of 0.204 Å and 0.257 Å respectively observed between all atoms in these pairs. Notably, R73 of chain B moved dramatically compared with R73 of chain C, as did Y161, Y154 and R157 of the α2 helix in chain B which rotated outwards to open up the ZAG groove. Measurement of the distances across the ZAG grooves of all six ZAG molecules in the ZAG:DAUDA asymmetric unit showed that the distance across the groove of chain B was the largest at 23.0 Å compared to ~20 Å for the other ZAG grooves (Table 2) including the previous ZAG:PEG structures [22, 44]. The more open groove, trapped in one subunit of this crystal form, demonstrates that the binding groove can undergo large conformational changes which would allow it to accommodate larger molecules.

Distinct DAUDA binding sites in the ZAG α1-α2 groove.

The coordination of the six groove-associated DAUDA molecules with ZAG were examined using LIGPLOT analyses of the ligand-protein interactions.

For the single DAUDA sites, the carboxylic head group of the DAUDA molecule occupying the ZAG groove of chain B formed two hydrogen bonds; one with R73 and the other with Thr169 (Figure 4A, third column, Figure 5). LIGPLOT showed that the rest of the DAUDA molecule made hydrophobic interactions with nonpolar atoms in Glu151, Trp148, Tyr117, Tyr154, Ile76, Cys166, Val153, Trp115, Tyr161, Phe101, Glu165 and Tyr12. In keeping with the similarity of the protein structures of ZAG chains E, F, A and D, the positions of the three DAUDA molecules in chains E, F and D were almost identical, albeit different, to the co-ordination of DAUDA in chain B (Figures 4B and 4C, third column, Figure 5). In all three cases, the hydroxyl group of Tyr117 formed a hydrogen bond with the sulfonyl group of DAUDA, the naphthalene ring of DAUDA formed hydrophobic interactions with nonpolar atoms in R73, and the fatty acid tail adopted a bent conformation with the carboxylic head projected out of the groove (Figures 4B and 4C, fourth column, Figure 5). For ZAG chain E, Ile76, Phe77, Trp115 and Trp148 formed hydrophobic interactions with DAUDA. For ZAG chain F, the almost identical Ile76, Phe77, Phe101, Trp115 and Trp148 residues made hydrophobic interactions with DAUDA (Figures 4B, third column, Figure 5). For ZAG chain A, Ile76, Phe77, Phe101, Trp115 and Trp148, Gln65 and Tyr154 made similar hydrophobic contacts with DAUDA (Figure 4C, third column, Figure 5).

For the two DAUDA molecules that tethered two ZAG grooves, the charged residues R73 and R157 and the polar residue Tyr117 of ZAG chains B and C formed hydrogen bonds with

the sulfonyl groups and/or carboxylate tails of two DAUDA molecules which bridged between the two grooves due to their close proximity in the crystal (Figure 7F).

Overall, our results show that ZAG binds DAUDA in two different conformations in the α1-α2 groove, and also that DAUDA was localised in different regions within its groove.

Oligomerisation of the ZAG:DAUDA complex in solution.
To determine if DAUDA binding induced the formation of ZAG dimers and tetramers in solution, as suggested by the crystal structure, AUC was performed with ZAG in the absence and presence of DAUDA.

Physiological concentrations of ZAG (6.2 μM) in the presence of 1:0, 1:1 and 1:10 molar ZAG:DAUDA equivalents were subjected to a high centrifugal force, and the sedimentation boundaries of each of ZAG and DAUDA were simultaneously but separately observed in real time at 280 nm (protein signal, Figure 8A,D) and 335 nm (DAUDA signal, Figures 8B,E) using the new multi wavelength absorbance optical system of the Optima AUC in phosphate buffered saline (PBS) and 4-(2-hydroxyethyl)-1-piperazineethanesulfonic acid (Hepes) buffers. PBS buffer was used to mimic physiological conditions while Hepes buffer was used to mimic the crystallisation conditions. The sedimentation boundaries were well fitted to size distribution analyses.

(i) The resulting *c(s)* analyses for ZAG in the absence of DAUDA at 280 nm revealed a major ZAG monomer peak at a mean $s_{20,w}$ value of 2.65 ± 0.06 S in PBS and 2.90 ± 0.15 S in Hepes (black, Figures 8C,F), similar to our previous determination of 2.83 ± 0.02 S for apo-ZAG in 10 mM Hepes, 137 mM NaCl, pH 7.4 [33]. Mass distribution *c(M)* plots showed that the ZAG monomer peaks corresponded to mean molecular masses of 31,600 ± 1,100 Da in PBS and 31,000 ± 2,400 Da in PBS, which agreed well with the sequence-determined theoretical mass of 32,276 Da. No other peaks were observed.

(ii) Following the addition of DAUDA in PBS buffer, the monomer $s_{20,w}$ values were unaffected (Table 3, Figure 7C). In Hepes buffer, the monomer $s_{20,w}$ values were reduced upon addition of DAUDA (Table 3, Figure 8F), this being attributed to buffer density changes upon addition of DAUDA in ethanol. The $s_{20,w}$ values generated from the sedimentation boundaries at 335 nm in PBS and Hepes followed the sedimentation of DAUDA. Because these were within experimental error of those generated from the sedimentation boundaries at 280 nm for ZAG itself (Table 3), this showed that DAUDA was bound to ZAG. Low amounts of 0.5-5.3% of dimer (4.43 – 5.12 S, corresponding to 66,942 Da) were seen for ZAG in the presence and absence of DAUDA (Figures 8C and 8F). However a small peak at 6.4 S was seen only in the presence of DAUDA at 335 nm (Figure 8F, bottom panel) which corresponded to the mass of tetramer ZAG. Taken together, the data showed that DAUDA was bound to ZAG at physiological ZAG concentrations, and migrated with ZAG predominantly as a monomer in solution. The presence of small dimer and tetramer peaks in the presence of DAUDA indicated that ZAG dimers and tetramers are able to form in solution, as seen in the crystal structure.

Higher concentrations of ZAG, equivalent to those used in the crystallization (155 μM ZAG; Figure 8G), in the presence of 1:1.6 molar ZAG:DAUDA equivalents were subjected to AUC, and the sedimentation of ZAG and DAUDA was observed in real time using interference optics (Figures 8G,H). The sedimentation boundaries were well fitted to give the *c(s)* analyses. Those for ZAG at high concentration revealed a ZAG monomer peak at a mean $s_{20,w}$ value of 2.69 ± 0.11 S in 20 mM Hepes pH 7.2 137 mM NaCl, similar to our observations at lower and more physiological ZAG concentrations. The intensity of the ZAG

monomer peak M was slightly increased by the addition of 248 μM (1:1.6) DAUDA (Figure 8I). While the *s* value appeared to be reduced upon addition of DAUDA (blue, Figure 8I), corrections for large changes in the buffer viscosity and density showed that the $s_{20,w}$ value was unaffected by the addition of DAUDA (Table 3). More visible peaks D corresponding to 2.3-3.6% dimeric ZAG, were apparent in the absence and presence of DAUDA. These support the existence in solution of the dimeric groove-tethered DAUDA complexes (chains B and C) seen in the crystal state. Lower amounts of 0.6-0.8% of ZAG corresponded approximately to trimer (5.8 S / 101 671 Da) and tetramer (6.4 S / 114 283 Da). The appearance of these small peaks makes it likely that these tetramers in solution constitute nucleation sites for lattice formation during crystallisation.

DISCUSSION

Here we report the first crystal structure of fatty acid binding to ZAG that revealed molecular details of multiple distinct and novel modes of lipid binding, namely within the ZAG α1-α2 groove and its tetrameric α3 β-barrel (Figure 9A). By this work, we show that ZAG has increased its previously known number of fatty acid binding sites. These details for the classic DAUDA binding at the α1-α2 groove showed that R73, I76 and F77 form hydrophobic interactions in ZAG:DAUDA chains E and F with the single DAUDA site, while R73, I76, F77 and Y154 form hydrophobic interactions in ZAG:DAUDA chain D. R73 forms a hydrogen bond, and I76, Y154, Y161 form hydrophobic interactions with ZAG:DAUDA chain B with the widened groove (Figure 7A). Interestingly, the α2-2 helix of ZAG (lower left helix, Figure 4A second column) moves in the complex, and not the α2-1 helix (lower right helix, Figure 4A second column) that moves in classic MHC-antigen complexes. Our results distinguish the discrete fatty acid binding sites seen in ZAG from those seen in plasma HSA and intracellular FABP, as well as from MHC-peptide complexes.

As a new observation relevant for ZAG function in solution, our ZAG:DAUDA crystal structure shows the ZAG α1-α2 groove of chain B has widened. The lipid binding immune class I MHC protein CD1e has a distance of 16 Å between groove helices, 2 Å wider than that of other CD1 family members [34]. CD1e is the only soluble member of the CD1 protein family. It binds two tailed bacterial lipids such as phosphatidylinositol and triacylated lipids and mediates lipid exchange/editing with CD1b [34]. The peptide binding immune class I MHC protein also contains a widened groove in the presence of bound peptide [45]. Its α2-1 helix swings downwards on binding to open up the groove [45]. The widened groove is stabilised by interactions with bound chaperone TABP binding protein [45]. A wide and exposed lipid binding site in ZAG may therefore enable binding of larger lipids, enhance the rate of lipid exchange, and / or stabilise its interaction with its receptor.

Our ZAG:DAUDA crystal structure confirmed our previous experiments that located the DAUDA binding site in the α1-α2 groove of ZAG. In these, fluorescence assays showed that PEG displaced bound DAUDA from the ZAG α1-α2 binding groove [22]. In agreement with this, our crystal structure showed that the positions of the DAUDA molecules in chains E, F and D overlapped with the positions of PEG seen in earlier ZAG crystal structures (Figure 7E). Furthermore, the three DAUDA molecules associated with ZAG chains E, F and D were each close to six residues R73, Y14, I76, F77, Y154 and Y161, that were previously identified using site directed mutagenesis to be critical for DAUDA binding by ZAG [31] (Figure 7B,C). This mutagenesis evidence supports our finding that the helices of the ZAG groove are flexible in solution, and enables the binding in solution of DAUDA in different locations and using different co-ordination geometries (Figure 7D).

LigPlot analyses showed that the dansyl group of DAUDA made variable amounts of hydrogen bonds and hydrophobic interactions with ZAG (Figure 5). In chain B, 33% of the DAUDA interactions arose from the dansyl group, while this increased to 63% for chain D, 67% for chain E, 71% for chain F. For the α3 domain, 43% occurred for each of chain A and chain B. The K_i for DHA upon titration with a pre-formed ZAG:DAUDA complex yielded a K_i value of 10 μM, which was unexpectedly larger and weaker than the K_d value of 0.51 μM for DAUDA binding to ZAG. These K_i calculations assumed that the DAUDA and DHA binding to ZAG were reversible with 1:1 stoichiometries for ZAG. Notably addition of ~ 60 fold excess of DHA to ZAG:DAUDA did not completely displace all the DAUDA from ZAG. While the DAUDA fluorescence emission intensity decreased, it was not red shifted and did not return to that of the original DAUDA fluorescence emission (Figure 2F). This suggested DAUDA bound to another ZAG site that was unaffected by DHA, in keeping with the multiple binding sites for DAUDA in our ZAG:DAUDA crystal structure. Our K_i binding model therefore only estimated the affinity of DHA binding to ZAG to be in the μM range. Previous studies detected no changes in the fluorescence emission of dansylamide upon incubation with ZAG [19]. Despite the high totals of LigPlot interactions, the ability of DHA to displace DAUDA makes it unlikely that the dansyl group contributes significantly to DAUDA binding.

For the novel observation of ZAG tetrameric α3 β-barrels, inspection showed that each was formed from four up-and-down four-stranded β-sheets stabilised by hydrogen bonds between the main chains at the edge of each β-sheets. Two of these bound four molecules of DAUDA in the unit cell (Figure 3B); these are evocative of the lipocalin fold which consists of an eight stranded antiparallel β-barrel enclosing an internal ligand-binding site [46]. Retinol, retinoic acid, arachidonic acid and steroids bind within the lipocalin fold. As such the lipocalins have been classified as extracellular transport proteins [46]. Our AUC analyses of ZAG in the absence and presence of DAUDA revealed that ZAG was predominantly a monomer in solution, but the detection of low amounts of tetramers (Figure 8) suggested that tetramers will form under the right conditions. The total buried surface area for each of the β-barrels formed by the AAAA, BBBB and CDEF α3 chains (Figure 3B) at the tetramer interfaces was 1170 ± 30 $Å^2$ per molecule (2340 $Å^2$ in total). These values were in excess of 800 $Å^2$ per molecule, showing that the observed β-barrels are able to form a stable protein-protein interaction in the right conditions [47]. Interestingly the DAUDA molecules do not bind to the α3 domain in the same place as the prolactin inducible protein (PIP) in its complex with ZAG [44].These DAUDA molecules were located at the four-stranded DEBA β-sheets of each α3 domain, formed from the β-strands D, E, B and A arranged in that order. Instead the β-strands D from each of the α3 domain and PIP form a hydrogen-bonded pair such that the two DEBA β-sheets form a continuous eight-stranded β-sheet to link the two proteins together. The ZAG-PIP complex does not therefore preclude formation of the ZAG-DAUDA complex (Figure 9B). The recombinant *E. coli* ZAG used in our experiments is not glycosylated. The crystal structure of human plasma ZAG shows the presence of glycans at three positions, namely Asn89 and Asn108 on the α1-α2 groove and Asn239 on the α3 domain (Figure 9C). Asn239 is conserved across species suggesting that glycosylation at this site may have a structural and or functional role. In the crystal structure of plasma ZAG, the glycan at Asn239 masks the DAUDA binding site in the α3 domain (Figure 9C). While the role of glycosylation in ZAG has not been directly tested in solution, this glycan chain in the α3 domain may be flexible enough to allow the binding of DAUDA to the α3 domain.

Functionally, the ZAG tetrameric α3 β-barrels may relate to cachexia. In this context, the presence of extra fatty acid binding sites in ZAG tetramers may comprise a mechanism to

transport excess free fatty acids released from adipocytes during lipolysis to muscle for storage in lipid droplets. Cachexia is a disorder characterized by loss of skeletal muscle mass with or without adipose tissue depletion which cannot be reversed by calorific feeding [48]. Ultimately its consequences are detrimental and can be fatal [48]. Cachexia occurs in association with cancer and other non-cancerous diseases including heart failure, kidney disease, COPD [49]. In cachexia, white adipose tissue depletion results from lipolysis and the generation of beige energy burning adipocytes [50]. Hyperlipidaemia is witnessed in patients with cancer cachexia [51, 52]. ZAG is upregulated in adipose tissue from human cachectic patients [53] and its expression correlates with circulating free fatty acid levels [12]Adipose tissue from mice bearing a cachexia inducing tumour showed shrunken adipocytes with modifications to the conformations of their cell membranes which contained excess mitochondria presumably to oxidise fatty acids [54]. However cachectic cancer patients also showed increases in amounts of lipids in their skeletal muscle compared with weight-stable cancer patients [55, 56]. Given that high plasma ZAG and fatty acid levels exist in cachexia, it is plausible that tetrameric ZAG may form to transport excess fatty acids released from adipocytes to muscle for storage in lipid droplets, thus contributing to adipose atrophy in cachexia. Further studies are required to determine the conditions in which ZAG tetramers form in solution and to clarify if DAUDA can bind to the ZAG α3 domain in solution.

In comparison with other lipid-binding proteins, HSA is the main plasma buffer for fatty acids at concentrations one hundred fold greater (0.6 mM; [57]) than ZAG (6.2 μM; [58]). HSA contains seven fatty acid binding sites [59] and binds saturated, monounsaturated and polyunsaturated fatty acids with nM affinities (K_d) [60]. Nine intracellular fatty acid binding proteins (FABP1 - FABP9) are expressed in human tissues with high rates of fatty acid uptake and lipid metabolism [23]. With the exception of FABP1 the remaining FABP2-FABP9 each have one fatty acid binding site, and bind saturated and unsaturated long-chain ($\geq {}^{14}C$) fatty acids with nM affinities [23]. FABP1 has two fatty acid binding sites and binds a range of hydrophobic compounds as well as fatty acids [23]. Our ZAG:DAUDA and HSA:DAUDA dissociation constants of 0.43 ± 0.15 μM (ZAG in PBS) and 0.51 ± 0.04 μM (ZAG in Hepes) and 0.11 ± 0.02 μM (HSA in PBS) are in keeping with previously reported measurements. Similar to HSA [30], FABP1 [61] and FABP2 [28], ZAG binds DAUDA with μM affinity [19, 31, 33] and within the range 0.08 μM to 1.5 μM (Table 4). The fact that ZAG binds DAUDA within a similar K_d range to HSA, FABP1 and FABP2 supports the likelihood that (one of) the physiological ligands of ZAG is a fatty acid. Polyunsaturated fatty acids (docosahexaenoic, eicosapentaenoic, linolenic, arachidonic and linoleic) were able to displace bound DAUDA from a preformed ZAG:DAUDA complex [19]. While we report an apparent dissociation constant (K_i) of 10 μM for DHA binding to a preformed ZAG:DAUDA complex here, the dissociation constants of ZAG for saturated, monounsaturated and polyunsaturated fatty acids (eicosapentaenoic, linolenic, arachidonic and linoleic) have yet to be measured.

The two co-ordination geometries of DAUDA bound to the ZAG groove (Figure 7D) have been seen in the crystal structures of HSA and FABP2, as well as the projection of the fatty acid carboxylate head out of the fatty acid binding site. Similar to the co-ordination of DAUDA to ZAG chain B (Figure 7A), the crystal structure of DAUDA in complex with intracellular intestinal fatty acid binding protein (FABP2) shows the DAUDA carboxylate group formed hydrogen bonds with Arg106 and Trp82 at the bottom of the binding cavity [28]. The other co-ordination of DAUDA to ZAG (Figures 7B,C) is similar to the co-ordinations of DAUDA to fatty acid binding sites 6 and 7 in HSA [29]. In both cases, a

positively charged amino acid (Lys212 in fatty acid binding site 6) and Arg218 (in site 7) interact with the DAUDA phenyl rings [29]. The projection of the fatty acid tail out of the groove and into the aqueous surroundings has been observed in oleate binding to human intracellular liver fatty acid binding protein (FABP1) [62] and in stearate binding by the immune MHC class I CD1c protein [63].

Overall we conclude that the observed multiple modes of fatty acid binding to a flexible α1-α2 binding groove and to the α3 β-barrel (orange spheres, Figure 9A) may confer a unique role for ZAG for the transport of fatty acids and larger lipids to be delivered to tissues that is not possible with HSA. This may be relevant to cachexia.

ACKNOWLEDGMENTS (including declarations of interest if any)
We thank Diamond Light support for access to beamlines I02 and I03 (Proposal number mx12342), Dr Gemma Harris and Dr David J. Scott (Research Complex at Harwell) for the use of a Beckman-Coulter Optima AUC instrument and Mr Maris Abele (University of Bedfordshire) for gel filtration chromatography measurements. LCMcD holds a purchasing and licensing agreement with the biotechnology company AdipoGen International.

AUTHOR CONTRIBUTION
A.M.L., H.Z., J.G.., S.J.P., A.R.C., and L.C.McD. designed and performed research, analyzed data and wrote the manuscript.

FUNDING: A.L., H.Z., S.J.P. and L.C.McD. were supported by Biotechnology and Biological Sciences Research Council BBSRC LIDO PhD studentship awards [grant number BB/M009513/1].

ACCESSION NUMBER: Coordinates and structure factors have been deposited at the Protein Data Bank with accession code 6R2U.

REFERENCES
1 Burgi, W. and Schmid, K. (1961) Preparation and properties of Zn-alpha 2-glycoprotein of normal human plasma. J. Biol. Chem. **236**, 1066-1074
2 Hale, L. P., Price, D. T., Sanchez, L. M., Demark-Wahnefried, W. and Madden, J. F. (2001) Zinc alpha-2-glycoprotein is expressed by malignant prostatic epithelium and may serve as a potential serum marker for prostate cancer. Clin. Cancer Res. **7**, 846-853
3 Tada, T., Ohkubo, I., Niwa, M., Sasaki, M., Tateyama, H. and Eimoto, T. (1991) Immunohistochemical localization of Zn-alpha 2-glycoprotein in normal human tissues. J. Histochem. Cytochem. **39**, 1221-1226
4 Elattar, S., Dimri, M. and Satyanarayana, A. (2018) The tumor secretory factor ZAG promotes white adipose tissue browning and energy wasting. FASEB J. **32**, 4727-4743
5 Xiao, X. H., Qi, X. Y., Wang, Y. D., Ran, L., Yang, J., Zhang, H. L., Xu, C. X., Wen, G. B. and Liu, J. H. (2018) Zinc alpha2 glycoprotein promotes browning in adipocytes. Biochem. Biophys. Res. Comms. **496**, 287-293
6 Mracek, T., Gao, D., Tzanavari, T., Bao, Y., Xiao, X., Stocker, C., Trayhurn, P. and Bing, C. (2010) Downregulation of zinc-{alpha}2-glycoprotein in adipose tissue and liver of obese ob/ob mice and by tumour necrosis factor-alpha in adipocytes. J. Endocrinol. **204**, 165-172
7 Selva, D. M., Lecube, A., Hernandez, C., Baena, J. A., Fort, J. M. and Simo, R. (2009) Lower zinc-alpha2-glycoprotein production by adipose tissue and liver in obese patients unrelated to insulin resistance. J. Clin. Endocrinol Metab. **94**, 4499-4507

8 Rolli, V., Radosavljevic, M., Astier, V., Macquin, C., Castan-Laurell, I., Visentin, V., Guigne, C., Carpene, C., Valet, P., Gilfillan, S. and Bahram, S. (2007) Lipolysis is altered in MHC class I zinc-alpha(2)-glycoprotein deficient mice. FEBS Lett. **581**, 394-400
9 Russell, S. T. and Tisdale, M. J. (2010) Antidiabetic properties of zinc-alpha2-glycoprotein in ob/ob mice. Endocrinol. **151**, 948-957
10 Russell, S. T., Hirai, K. and Tisdale, M. J. (2002) Role of beta3-adrenergic receptors in the action of a tumour lipid mobilizing factor. British J Cancer. **86**, 424-428
11 Pelletier, C. C., Koppe, L., Alix, P. M., Kalbacher, E., Croze, M. L., Hadj-Aissa, A., Fouque, D., Guebre-Egziabher, F. and Soulage, C. O. (2014) The relationship between renal function and plasma concentration of the cachectic factor zinc-alpha2-glycoprotein (ZAG) in adult patients with chronic kidney disease. PloS One. **9**, e103475
12 Tedeschi, S., Pilotti, E., Parenti, E., Vicini, V., Coghi, P., Montanari, A., Regolisti, G., Fiaccadori, E. and Cabassi, A. (2012) Serum adipokine zinc alpha2-glycoprotein and lipolysis in cachectic and noncachectic heart failure patients: relationship with neurohormonal and inflammatory biomarkers. Metab.: clinical and experimental. **61**, 37-42
13 Xu, L., Yu, W., Niu, M., Zheng, C., Qu, B., Li, Y., Wang, J., Huang, P., Wang, O. and Gong, F. (2017) Serum ZAG Levels Were Associated with eGFR Mild Decrease in T2DM Patients with Diabetic Nephropathy. Int J Endocrinol. **2017**, 5372625
14 Zhu, H. J., Wang, X. Q., Pan, H., Gong, F. Y., Zhang, D. X., Li, N. S., Wang, L. J. and Yang, H. B. (2014) Serum Levels of the Adipokine Zinc- alpha 2-glycoprotein Are Decreased in Patients with Hypertension. ISRN Endocrinol. **2014**, 374090
15 Boersema, P. J., Geiger, T., Wisniewski, J. R. and Mann, M. (2013) Quantification of the N-glycosylated secretome by super-SILAC during breast cancer progression and in human blood samples. Mol Cell Proteomics :. **12**, 158-171
16 Whelan, S. A., He, J., Lu, M., Souda, P., Saxton, R. E., Faull, K. F., Whitelegge, J. P. and Chang, H. R. (2012) Mass spectrometry (LC-MS/MS) identified proteomic biosignatures of breast cancer in proximal fluid. J Proteome Res. **11**, 5034-5045
17 Xue, Y. M., Yu, F. D., Yan, D. W., Cui, F. F., Tang, H. M., Wang, X. L., Chen, J., Lu, H. J., Zhao, S. L. and Peng, Z. H. (2015) Zinc-alpha-2-Glycoprotein: A Candidate Biomarker for Colon Cancer Diagnosis in Chinese Population. Int J Mol Sci. **16**, 691-703
18 Zhu, H. J., Liu, M. J., Zhang, N. R., Pan, H., Lin, G. L., Li, N. S., Wang, L. J., Yang, H. B., Yan, K. M. and Gong, F. Y. (2018) Circulating and Adipose Tissue mRNA Levels of Zinc-alpha 2-Glycoprotein, Leptin, High-Molecular-Weight Adiponectin, and Tumor Necrosis Factor-Alpha in Colorectal Cancer Patients With or Without Obesity. Front Endocrinol. **9**
19 Kennedy, M. W., Heikema, A. P., Cooper, A., Bjorkman, P. J. and Sanchez, L. M. (2001) Hydrophobic ligand binding by Zn-alpha 2-glycoprotein, a soluble fat-depleting factor related to major histocompatibility complex proteins. J Biol Chem. **276**, 35008-35013
20 Hassan, M. I., Kumar, V., Singh, T. P. and Yadav, S. (2008) Purification and characterization of zinc alpha2-glycoprotein-prolactin inducible protein complex from human seminal plasma. J Sep Sci. **31**, 2318-2324
21 Sanchez, L. M., Chirino, A. J. and Bjorkman, P. (1999) Crystal structure of human ZAG, a fat-depleting factor related to MHC molecules. Science. **283**, 1914-1919
22 Delker, S. L., West, A. P., Jr., McDermott, L., Kennedy, M. W. and Bjorkman, P. J. (2004) Crystallographic studies of ligand binding by Zn-alpha2-glycoprotein. J Struct Biol. **148**, 205-213
23 Storch, J. and McDermott, L. (2009) Structural and functional analysis of fatty acid-binding proteins. J Lipid Res. **50 Suppl**, S126-131
24 McDermott, L., Moore, J., Brass, A., Price, N. C., Kelly, S. M., Cooper, A. and Kennedy, M. W. (2001) Mutagenic and chemical modification of the ABA-1 allergen of the

nematode Ascaris: consequences for structure and lipid binding properties. Biochemistry. **40**, 9918-9926
25 Moore, J., McDermott, L., Price, N. C., Kelly, S. M., Cooper, A. and Kennedy, M. W. (1999) Sequence-divergent units of the ABA-1 polyprotein array of the nematode Ascaris suum have similar fatty-acid- and retinol-binding properties but different binding-site environments. Biochem J. **340 (Pt 1)**, 337-343
26 Zhan, B., Arumugam, S., Kennedy, M. W., Tricoche, N., Lian, L. Y., Asojo, O. A., Bennuru, S., Bottazzi, M. E., Hotez, P. J., Lustigman, S. and Klei, T. R. (2018) Ligand binding properties of two Brugia malayi fatty acid and retinol (FAR) binding proteins and their vaccine efficacies against challenge infection in gerbils. PLoS Negl Trop Dis. **12**, e0006772
27 Kennedy, M. W., Scott, J. C., Lo, S., Beauchamp, J. and McManus, D. P. (2000) Sj-FABPc fatty-acid-binding protein of the human blood fluke Schistosoma japonicum: structural and functional characterization and unusual solvent exposure of a portal-proximal tryptophan residue. Biochem J. **349**, 377-384
28 Patil, R., Laguerre, A., Wielens, J., Headey, S. J., Williams, M. L., Hughes, M. L., Mohanty, B., Porter, C. J. and Scanlon, M. J. (2014) Characterization of two distinct modes of drug binding to human intestinal fatty acid binding protein. ACS Chem Biol. **9**, 2526-2534
29 Wang, Y., Luo, Z., Shi, X., Wang, H., Nie, L. and Huang, M. (2011) A fluorescent fatty acid probe, DAUDA, selectively displaces two myristates bound in human serum albumin. Prot.Sci. **20**, 2095-2101
30 Wilton, D. C. (1990) The fatty acid analogue 11-(dansylamino)undecanoic acid is a fluorescent probe for the bilirubin-binding sites of albumin and not for the high-affinity fatty acid-binding sites. Biochem J. **270**, 163-166
31 McDermott, L. C., Freel, J. A., West, A. P., Bjorkman, P. J. and Kennedy, M. W. (2006) Zn-alpha2-glycoprotein, an MHC class I-related glycoprotein regulator of adipose tissues: modification or abrogation of ligand binding by site-directed mutagenesis. Biochemistry. **45**, 2035-2041
32 Kumar, A. A., Hati, D., Thaker, T. M., Miah, L., Cunningham, P., Domene, C., Bui, T. T., Drake, A. F. and McDermott, L. C. (2013) Strong and weak zinc binding sites in human zinc-alpha2-glycoprotein. FEBS Lett. **587**, 3949-3954
33 Zahid, H., Miah, L., Lau, A. M., Brochard, L., Hati, D., Bui, T. T., Drake, A. F., Gor, J., Perkins, S. J. and McDermott, L. C. (2016) Zinc-induced oligomerization of zinc alpha2 glycoprotein reveals multiple fatty acid-binding sites. Biochem J. **473**, 43-54
34 Garcia-Alles, L. F., Giacometti, G., Versluis, C., Maveyraud, L., de Paepe, D., Guiard, J., Tranier, S., Gilleron, M., Prandi, J., Hanau, D., Heck, A. J., Mori, L., De Libero, G., Puzo, G., Mourey, L. and de la Salle, H. (2011) Crystal structure of human CD1e reveals a groove suited for lipid-exchange processes. PNAS. **108**, 13230-13235
35 Gill, S. C. and von Hippel, P. H. (1989) Calculation of protein extinction coefficients from amino acid sequence data. Anal. Biochem. **182**, 319-326
36 Cer, R. Z., Mudunuri, U., Stephens, R. and Lebeda, F. J. (2009) IC50-to-Ki: a web-based tool for converting IC50 to Ki values for inhibitors of enzyme activity and ligand binding. Nucleic Acids Res. **37**, W441-445
37 McCoy, A. J., Grosse-Kunstleve, R. W., Adams, P. D., Winn, M. D., Storoni, L. C. and Read, R. J. (2007) Phaser crystallographic software. J Appl Crystallogr.. **40**, 658-674
38 Padilla, J. E. and Yeates, T. O. (2003) A statistic for local intensity differences: robustness to anisotropy and pseudo-centering and utility for detecting twinning. Acta Crystallogr D Biol Crystallogr. **59**, 1124-1130
39 Winn, M. D., Ballard, C. C., Cowtan, K. D., Dodson, E. J., Emsley, P., Evans, P. R., Keegan, R. M., Krissinel, E. B., Leslie, A. G., McCoy, A., McNicholas, S. J., Murshudov, G.

N., Pannu, N. S., Potterton, E. A., Powell, H. R., Read, R. J., Vagin, A. and Wilson, K. S. (2011) Overview of the CCP4 suite and current developments. Acta Crystallogr D Biol Crystallogr. **67**, 235-242
40 Afonine, P. V., Grosse-Kunstleve, R. W., Echols, N., Headd, J. J., Moriarty, N. W., Mustyakimov, M., Terwilliger, T. C., Urzhumtsev, A., Zwart, P. H. and Adams, P. D. (2012) Towards automated crystallographic structure refinement with phenix.refine. Acta Crystallogr D Biol Crystallogr. **68**, 352-367
41 Wallace, A. C., Laskowski, R. A. and Thornton, J. M. (1995) LIGPLOT: a program to generate schematic diagrams of protein-ligand interactions. Prot. Eng. **8**, 127-134
42 Laue T. M., S. B. D., Ridgeway T. M., Pelletier S. L. . (1992) Analytical Ultracentrifugation in Biochemistry and Polymer Science. Royal Society of Chemistry, Cambridge, UK.

43 Karplus, P. A. and Diederichs, K. (2015) Assessing and maximizing data quality in macromolecular crystallography. Curr Opin Struct Biol.. **34**, 60-68
44 Hassan, M. I., Bilgrami, S., Kumar, V., Singh, N., Yadav, S., Kaur, P. and Singh, T. P. (2008) Crystal structure of the novel complex formed between zinc alpha2-glycoprotein (ZAG) and prolactin-inducible protein (PIP) from human seminal plasma. J J Mol Biol. **384**, 663-672
45 Thomas, C. and Tampe, R. (2017) Structure of the TAPBPR-MHC I complex defines the mechanism of peptide loading and editing. Science. **358**, 1060-1064
46 Flower, D. R. (1996) The lipocalin protein family: structure and function. Biochem J. **318 (Pt 1)**, 1-14
47 Rupp, B. (2010) Biomolecular crystallogrpahy: principle, practice and application to structural biology. Garland Science, New York, U.S.A and Abingdon, U.K.
48 Fearon, K., Strasser, F., Anker, S. D., Bosaeus, I., Bruera, E., Fainsinger, R. L., Jatoi, A., Loprinzi, C., MacDonald, N., Mantovani, G., Davis, M., Muscaritoli, M., Ottery, F., Radbruch, L., Ravasco, P., Walsh, D., Wilcock, A., Kaasa, S. and Baracos, V. E. (2011) Definition and classification of cancer cachexia: an international consensus. Lancet Oncol. **12**, 489-495
49 Lok, C. (2015) Cachexia: The last illness. Nature. **528**, 182-183
50 Dalal, S. (2019) Lipid metabolism in cancer cachexia. Ann Palliat Med. **8**, 13-23
51 Das, S. K. and Hoefler, G. (2013) The role of triglyceride lipases in cancer associated cachexia. Trends Mol Med. **19**, 292-301
52 Shaw, J. H. and Wolfe, R. R. (1987) Fatty acid and glycerol kinetics in septic patients and in patients with gastrointestinal cancer. The response to glucose infusion and parenteral feeding. Ann Surg. **205**, 368-376
53 Mracek, T., Stephens, N. A., Gao, D., Bao, Y., Ross, J. A., Ryden, M., Arner, P., Trayhurn, P., Fearon, K. C. and Bing, C. (2011) Enhanced ZAG production by subcutaneous adipose tissue is linked to weight loss in gastrointestinal cancer patients. Br J Cancer. **104**, 441-447
54 Bing, C., Russell, S., Becket, E., Pope, M., Tisdale, M. J., Trayhurn, P. and Jenkins, J. R. (2006) Adipose atrophy in cancer cachexia: morphologic and molecular analysis of adipose tissue in tumour-bearing mice. Br J Cancer. **95**, 1028-1037
55 Stephens, N. A., Skipworth, R. J., Macdonald, A. J., Greig, C. A., Ross, J. A. and Fearon, K. C. (2011) Intramyocellular lipid droplets increase with progression of cachexia in cancer patients. J Cachexia Sarcopenia Muscle. **2**, 111-117
56 Weber, M. A., Krakowski-Roosen, H., Schroder, L., Kinscherf, R., Krix, M., Kopp-Schneider, A., Essig, M., Bachert, P., Kauczor, H. U. and Hildebrandt, W. (2009)

Morphology, metabolism, microcirculation, and strength of skeletal muscles in cancer-related cachexia. Acta Oncol. **48**, 116-124
57 Peters Jr., T. (1995) All about Albumin: Biochemistry, Genetics and Medical Applications. Academic Press, San Diego
58 Hale, L. P. (2002) Zinc alpha-2-glycoprotein regulates melanin production by normal and malignant melanocytes. J Invest Dermatol. **119**, 464-470
59 Bhattacharya, A. A., Grune, T. and Curry, S. (2000) Crystallographic analysis reveals common modes of binding of medium and long-chain fatty acids to human serum albumin. J Mol Biol. **303**, 721-732
60 Richieri, G. V., Anel, A. and Kleinfeld, A. M. (1993) Interactions of long-chain fatty acids and albumin: determination of free fatty acid levels using the fluorescent probe ADIFAB. Biochemistry. **32**, 7574-7580
61 Maatman, R. G., van Moerkerk, H. T., Nooren, I. M., van Zoelen, E. J. and Veerkamp, J. H. (1994) Expression of human liver fatty acid-binding protein in Escherichia coli and comparative analysis of its binding characteristics with muscle fatty acid-binding protein. Biochim Biophys Acta. **1214**, 1-10
62 Cai, J., Lucke, C., Chen, Z., Qiao, Y., Klimtchuk, E. and Hamilton, J. A. (2012) Solution structure and backbone dynamics of human liver fatty acid binding protein: fatty acid binding revisited. Biophys. J. **102**, 2585-2594
63 Mansour, S., Tocheva, A. S., Cave-Ayland, C., Machelett, M. M., Sander, B., Lissin, N. M., Molloy, P. E., Baird, M. S., Stubs, G., Schroder, N. W., Schumann, R. R., Rademann, J., Postle, A. D., Jakobsen, B. K., Marshall, B. G., Gosain, R., Elkington, P. T., Elliott, T., Skylaris, C. K., Essex, J. W., Tews, I. and Gadola, S. D. (2016) Cholesteryl esters stabilize human CD1c conformations for recognition by self-reactive T cells. PNAS. **113**, E1266-1275

TABLES

Table 1. Crystallographic and refinement statistics for bacterial-expressed human ZAG complexed with C_{11} DAUDA as ligand

Parameters	**Values**
Space group	I4
Unit cell dimensions (Å)	a = b = 167.01Å; c = 204.95Å
Matthews coefficient	3.70
Data statistics	
Resolution (Å)	77.40 - 2.49
Number of measurements	1,496,504
Number of unique reflections	98,002
Completeness (%)	100.0 (99.2) [a]
Multiplicity of higher resolution shell	15.6
Multiplicity of outer shell (2.53 – 2.49 Å)	15.6
Overall multiplicity	15.3
R_{pim} (%) [b]	0.276 (1.205)
(I)/σ(I)	10.0 (1.0)
Half-set correlation CC(1/2)	0.995 (0.298)
Refinement statistics [b]	
R_{work} / R_{free} (%) [c]	0.170 / 0.212
Number of protein atoms	13792
Number of water atoms	110
Number of ligand atoms	240
Number of reflections	95132
Mean overall *B* value (Å^2)	62.751
Data used in refinement	
Resolution range (Å^2)	77.399 – 2.490
Percentage observed	99.980
Percentage of free reflections	2.758
Root mean square deviations from ideal geometry	
Bond lengths (Å)	0.55
Bond angles (degrees)	0.75
Ramachandran plot	
Number in favored regions (%)	92.5
Number in allowed regions (%)	7.3
Outliers (%)	0.2
Twinning	0.637 for h, k, l 0.363 for –h, k, -l

[a] Values in parentheses are for the highest resolution shell.

[b] Precision-indicating merging *R* factor, $R_{pim} = \Sigma_h (1/(n_h - 1))^{½} \Sigma_1 | I_{h1} - \langle I_h \rangle | / \Sigma_h \Sigma_l \langle I_h \rangle$, where n_h is the number of observations of reflection *h*, I_{hl} is the *l*th observation of reflection *h*, and $\langle I_h \rangle$ is the average intensity for all observations *l* of reflection *h*.

[c] R_{work} and $R_{free} = \Sigma \mid\mid F_{obs}| - |F_{calc}|| / \Sigma \mid F_{obs} \mid \times 100$ for 95% of the recorded data (R_{work}) and 5% of the data (R_{free}). F_{obs} is the observed structure factor amplitude, and F_{calc} is the calculated structure factor amplitude.

Table 2. Distance between the Cα atoms of the ZAG groove residues Asp75 on helix α1 and Val153 on helix α2

Polypeptide chain	Separation distance (Å)
ZAG chain A	20.9
ZAG: DAUDA chain B	23.0
ZAG chain C	20.1
ZAG:DAUDA chain D	19.6
ZAG:DAUDA chain E	20.3
ZAG:DAUDA chain F	19.1
ZAG:PEG (1T7V)	20.5
ZAG:PEG (3ES6)	20.5

Table 3. Sedimentation coefficients $s_{20,w}$ values for ZAG in the absence and presence of DAUDA

	$s_{20,w}$				
	PBS pH 7.4 (S)		20 mM Hepes pH 7.6 (S)		20 mM Hepes 137 mM NaCl pH 7.2 (S)
ZAG:DAUDA	280 nm	335 nm	280 nm	335 nm	Interference
1:0	2.65 ± 0.06		2.90 ± 0.15		2.69 ± 0.11
1:1	2.57 ± 0.09	2.54 ± 0.29	2.58 ± 0.08	2.59 ± 0.38	
1:1.6					2.78 ± 0.10*
1:10	2.64 ± 0.14	2.70 ± 0.07	2.69 ± 0.10	2.78 ± 0.31	

*Note this $s_{20,w}$ value does not correspond to the sedimentation coefficient (S) plotted in Figure 5I. The *c(s)* plot does not include corrections for buffer viscosity and density which were altered upon addition of DAUDA. DAUDA was added in 100% ethanol to give a final ethanol concentrations of 9% in the sample cell. 9% ethanol was subsequently added to the buffer cell.

Table 4. Dissociation constants K_d for DAUDA binding to human extracellular and intracellular fatty acid binding proteins

Protein	Method	Buffer	n	K_d (µM±SD)	Reference
ZAG	ITC	PBS	1	1.5	[19]
ZAG	Fluorescence	PBS	1	0.73 ± 0.08	[31]
ZAG	Fluorescence	10 mM Hepes pH 7.4 137 mM NaCl	1	0.11 ± 0.01	[33]
HSA	Fluorescence	0.1M potassium phosphate pH 7.4	3	0.08	[30]
FABP2	Fluorescence	20 mM MES pH 5.5, 50 mM NaCl	1	0.3	[28]
FABP2	ITC	20 mM Hepes pH 8, 50 mM NaCl, 0.5 mM EDTA),	1.2	0.36	[28]
FABP1	Fluorescence	10 mM Tris-HCl pH 8	*	0.17 ± 0.01	[61]

Key: HSA, human serum albumin; FABP2, intestinal fatty acid binding protein; FABP1, liver fatty acid binding protein; n, number of binding sites; *, not disclosed

FIGURE LEGENDS

Figure 1. Recombinant *E.coli* ZAG purification and crystals of the ZAG:DAUDA complex. A, Preparative size-exclusion chromatography of refolded ZAG in PBS buffer; (inset) Calibration of the Superdex 75 size exclusion gel filtration column using five standard proteins of known MW. ZAG had an elution volume of 88 ml generating a K_{av} value of 0.57 and estimated MW of 33 787 Da (represented by the dotted line). **B**, Non-reducing gradient 4 – 20% SDS PAGE of 22 μM, 11 μM and 4.4 μM ZAG. **C**, Chemical structure of the dansylated fluorescent C_{11} fatty acid probe 11-(dansylamino)undecanoic acid (DAUDA). The fatty acid carboxylate group is highlighted in red, the fatty acid carbon chain is highlighted in green, the dansyl sulfonyl group is highlighted in blue and the dansyl napthalene group is highlighted in dark blue. DAUDA has a maximum absorbance wavelength of 335 nm. **D**, Crystals of the ZAG:DAUDA complex used for the structure determination. Crystals were prepared using a 2 μl hanging drop containing 155 μM ZAG, 230 μM DAUDA (1:1.5 ZAG:DAUDA), 10% methanol (v/v), 58 mM Hepes pH 7.25, 0.008% NaN_3, 0.65 M ammonium sulfate and a buffer reservoir containing 1.3 M ammonium sulfate, 20 mM Hepes pH 7.59.

Figure 2. DAUDA binding function of ZAG. Fluorescence emission spectra at the excitation wavelength of 345 nm of 1 μM DAUDA in PBS and Hepes buffers upon sequential additions of **A, B** ZAG and **C** albumin (HSA). **D**, The binding curves of DAUDA with ZAG in PBS and Hepes buffers, and of albumin in PBS buffer. **E**, Fluorescence emission spectra of a pre-formed 0.9 μM DAUDA:0.87 μM ZAG complex upon sequential additions of docosahexaenoic acid (DHA) in PBS. All fluorescence spectra were corrected for the effects of dilution and solvent Raman scattering. **F,** The binding curve representing ZAG:DHA complex formation.

Figure 3. The ZAG:DAUDA asymmetric unit and crystal packing A, The crystallographic ZAG:DAUDA asymmetric unit contained six ZAG and eight DAUDA molecules. Six DAUDA molecules were bound at the ZAG α1-α2 domain binding groove. The remaining two DAUDA molecules were associated with the α3 domains of chains A and B. **B**, Rotation of the ZAG:DAUDA asymmetric unit by 45° and display of symmetry equivalent molecules revealed β-barrel structures within the crystal lattice, formed from the association of four chain A α3 domains (lower), four chain B α3 domains (upper) and four α3 domains from chains C, D, E and F. Four DAUDA molecules were located inside the chains AAAA and BBBB β-barrel structures while the chains CDEF β-barrel was empty.

Figure 4. The fitted electron densities of DAUDA and movement of the ZAG groove. From left to right: **A**, Electron density from a composite omit map for three DAUDA molecules located in chains B and C, the superimposition of chains B and C and their three DAUDA molecules (black, dark grey, and light grey), a close-up view of the α1-α2 domain binding groove from chains B showing residues involved in co-ordinating DAUDA (red and blue), and a lateral view of the ZAG groove chain B (light grey). **B**, Electron density fits for DAUDA located in chains E and F, the superimposition of chains E and F and their corresponding DAUDA molecules (dark grey), a close-up view of the DAUDA binding pocket in chain F and highlighting residues involved in ZAG-DAUDA co-ordination (red and blue), and a lateral view of the groove of chain E to show the extension of the DAUDA carboxylic acid group out of the groove. **C**, The electron density fit for DAUDA located in chain D, the superimposition of chains A and D, a close-up view of the α1-α2 domain binding groove from chains D showing residues involved in co-ordinating DAUDA (red and blue)

and a lateral view of the groove of chain D to show the extension of the DAUDA carboxylic acid group out of the groove. Electron densities were generated from a composite ZAG-DAUDA omit map contoured to 1.0σ.

Figure 5. LigPlot interaction analyses of DAUDA with ZAG. DAUDA and non-ligand residues are shown in ball and stick representations. Hydrogen bonds are represented by dashed green lines with bond lengths shown in Angstroms. Hydrophobic contacts are represented by the red arcs with spokes pointing towards the ligand atoms they contact. In the LigPlot interactions of α1α2 Chain B, 11d303 denotes one of the DAUDA molecules linking chains B and C.

Figure 6. The locations of the eight DAUDA molecules in ZAG A, Four DAUDA molecules were associated with chains B and C (pink), where two DAUDA link the α1-α2 domains of chains B and C, one DAUDA was located in the α1-α2 domain groove of chain B, and the fourth DAUDA was associated with the α3 domain of chain B. **B**, Two DAUDA molecules are associated with chains A and D (yellow). One was buried in the α1-α2 domain binding groove of chain D while the second was associated with the α3 domain of chain A. **C**, Chains E and F (blue) each contained one DAUDA bound within the α1-α2 domain binding groove.

Figure 7. Distinct DAUDA binding sites in the ZAG groove. A, B, C, Views of four ZAG α1-α2 domain binding grooves (chains B, E, F and D), each of which contained a single bound DAUDA molecule. The positions of each DAUDA molecule (light and dark grey) are shown relative to groove residues Y14, F77, I76, Y154, Y161 and R73 (yellow). Sidechains highlighted in yellow denote those that abrogate DAUDA binding to ZAG when mutated to alanine, as previously shown [31]. **D**, Superimposition of chains B, E, F and D and their corresponding DAUDA molecules highlighting the two different positions of four DAUDA molecules bound within the ZAG groove. **E**, The two binding conformations of polyethylene glycol (PEG: grey/orange) in baculovirus-expressed ZAG (PDB code: 1T7V) and seminal ZAG-prolactin inducible protein (PIP) complex (PDB code: 3ES6). **F**, Views of the ZAG grooves of chains B and C and highlighting the positions of two DAUDA molecules (grey and dark grey) that cross-link the grooves of chains B and C.

Figure 8. Sedimentation velocity of ZAG with C_{11} DAUDA in PBS and Hepes buffer. Multiwavelength absorbance sedimentation data and boundary fits are shown for the 6.2 μM 1:1 ZAG:DAUDA complex in **A, B**, PBS and **D, E**, Hepes buffer at wavelengths of 280 nm (protein) and 335 nm (DAUDA). For clarity only every fifth scan is shown in the fitted data plots. These resulted in the sedimentation coefficient *c(s)* distribution analyses of 6.2 μM ZAG, 1:1 ZAG:DAUDA and 1:10 ZAG: DAUDA complexes at 280 nm and 335 nm in **C** PBS and **F** Hepes buffer respectively. Two further sedimentation data and boundary fits at high concentration are shown for **G** 155 μM apo-ZAG and **H,** 155 μM 1:1.6 ZAG:DAUDA complex in 20 mM Hepes, 137 mM NaCl buffer using interference optics. For clarity only every second scan is shown in the fitted data plots. **I**, The sedimentation coefficient *c(s)* distribution analyses of 155 μM ZAG (black) and 1:1.6 ZAG:DAUDA complex (blue) in 20 mM Hepes, 137 mM NaCl buffer. The sedimentation coefficient (S) values plotted in **I** were not corrected for buffer viscosity and density which were altered upon addition of DAUDA. When corrections for changes in buffer viscosity and density are included the $s_{20,w}$ values for apo ZAG and ZAG:DAUDA are very similar (Table 3). In panels C, F and I, M denotes monomer, D denotes dimer and T denotes tetramer.

Figure 9. Summary of the ZAG-DAUDA, ZAG-PIP and glycosylated plasma ZAG crystal structures. A, side-on view of chain B of ZAG to show four DAUDA molecules bound to this. The three DAUDA molecules in the α1-α2 groove and one associated with the α3 domain of chain B are indicated as orange spheres. The DEBA β-sheet in the α3 domain is denoted as lettered, with the GFC β-sheet behind this as viewed. **B**, the same side-on view is shown for the ZAG-PIP complex (PDB code 3ES6). **C,** the same side-on view is shown for human plasma ZAG (PDB code 1ZAG) which is glycosylated at Asn89 and Asn108 on the α1-α2 groove and Asn239 on the α3 domain.

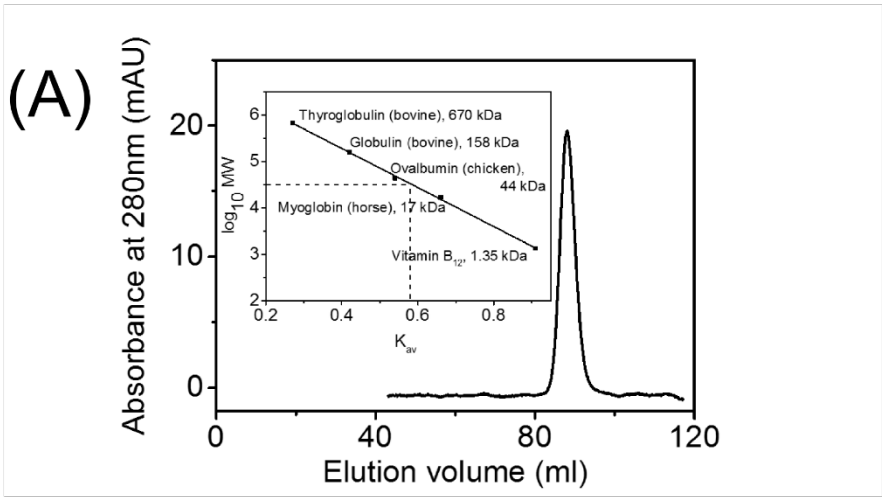
(A)
Absorbance at 280nm (mAU)
Elution volume (ml)
Thyroglobulin (bovine), 670 kDa
Globulin (bovine), 158 kDa
Ovalbumin (chicken), 44 kDa
Myoglobin (horse), 17 kDa
Vitamin B12, 1.35 kDa
log10 MW
Kav

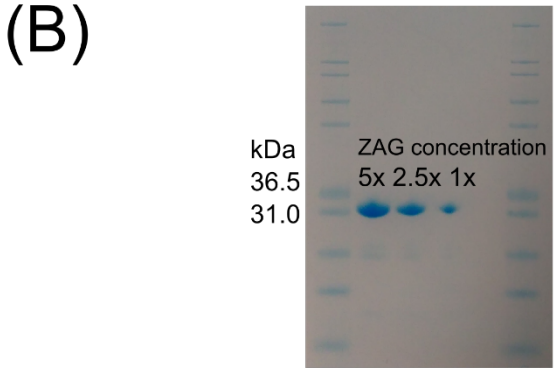
(B)
kDa
36.5
31.0
ZAG concentration
5x 2.5x 1x

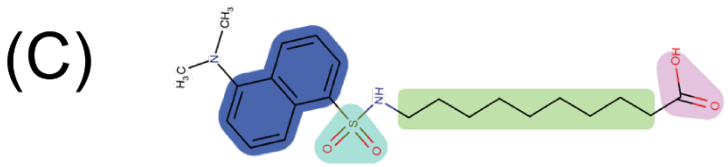
(C)

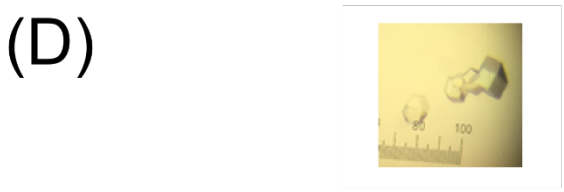
(D)

FIGURE 1

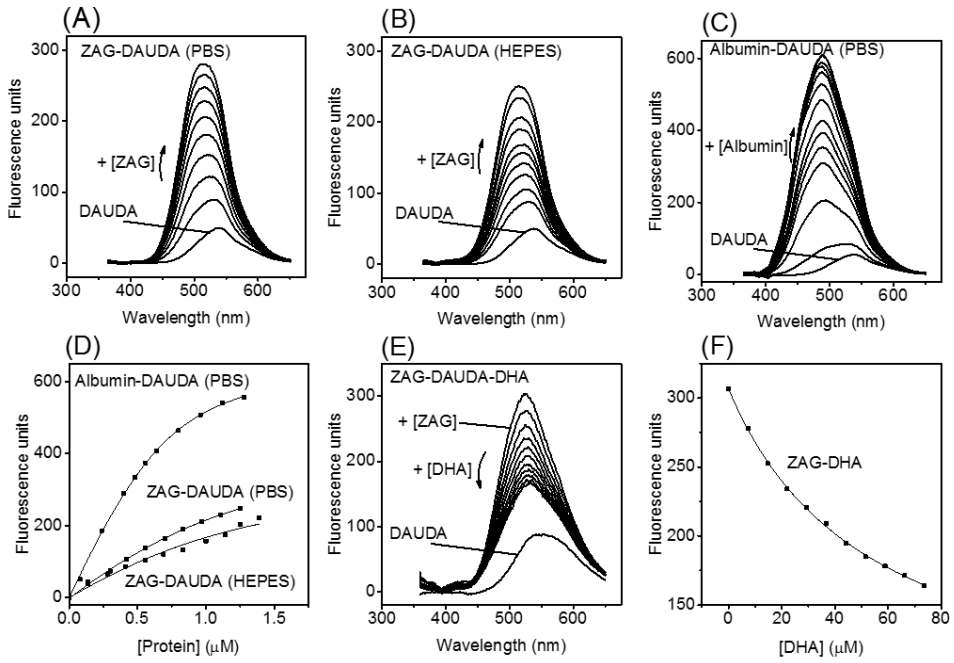
(A)
ZAG-DAUDA (PBS)
+ [ZAG]
DAUDA
Fluorescence units
Wavelength (nm)
(B)
ZAG-DAUDA (HEPES)
+ [ZAG]
DAUDA
Fluorescence units
Wavelength (nm)
(C)
Albumin-DAUDA (PBS)
+ [Albumin]
DAUDA
Fluorescence units
Wavelength (nm)
(D)
Albumin-DAUDA (PBS)
ZAG-DAUDA (PBS)
ZAG-DAUDA (HEPES)
Fluorescence units
[Protein] (μM)
(E)
ZAG-DAUDA-DHA
+ [ZAG]
+ [DHA]
DAUDA
Fluorescence units
Wavelength (nm)
(F)
ZAG-DHA
Fluorescence units
[DHA] (μM)

FIGURE 2

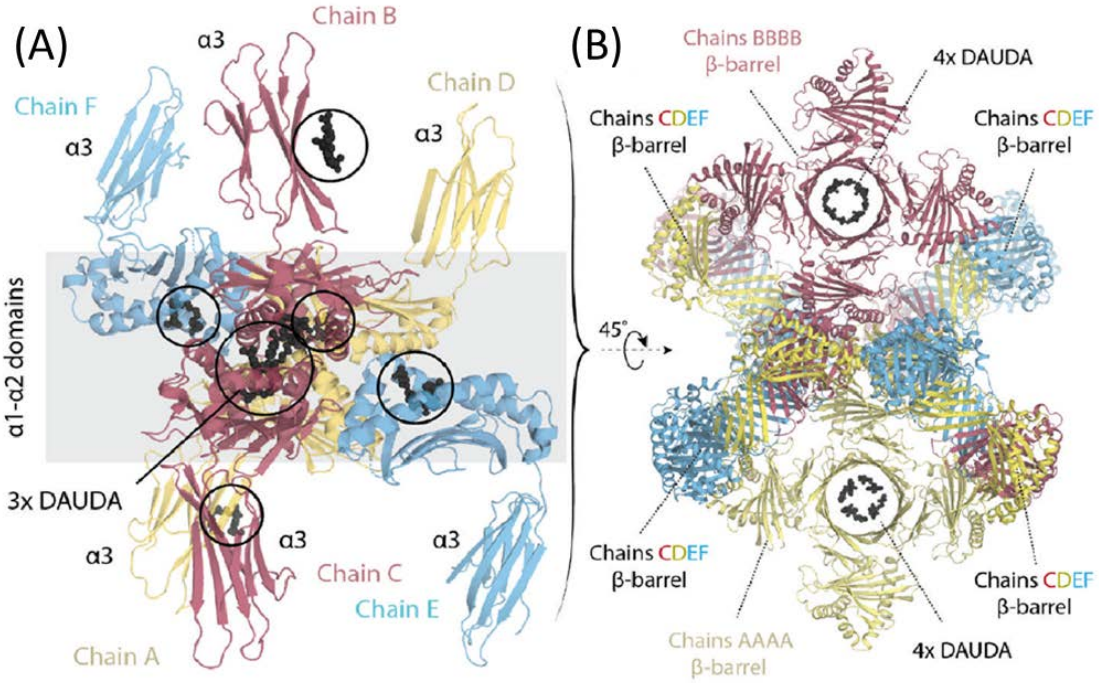
(A)
Chain B
α3
Chain D
Chain F
α3
α3
α1-α2 domains
3x DAUDA
α3
α3
α3
Chain C
Chain E
Chain A
(B)
Chains BBBB
β-barrel
4x DAUDA
Chains CDEF
β-barrel
Chains CDEF
β-barrel
45°
Chains CDEF
β-barrel
Chains CDEF
β-barrel
Chains AAAA
β-barrel
4x DAUDA

FIGURE 3

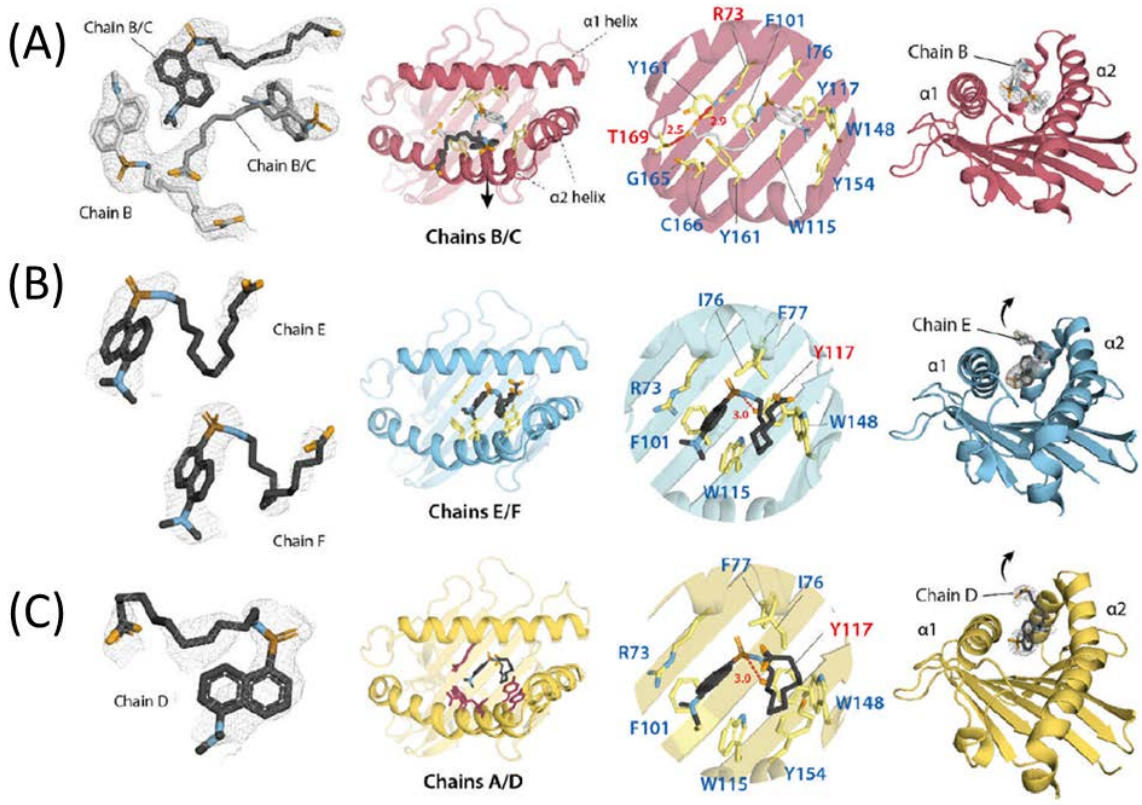
(A)
Chain B/C
Chain B/C
Chain B
α1 helix
α2 helix
Chains B/C
R73
E101
I76
Y161
Y117
T169
2.5
2.9
W148
G165
Y154
C166
Y161
W115
Chain B
α2
α1
(B)
Chain E
Chain F
Chains E/F
I76
F77
Y117
R73
3.0
W148
F101
W115
Chain E
α2
α1
(C)
Chain D
Chains A/D
F77
I76
Y117
R73
3.0
W148
F101
W115
Y154
Chain D
α2
α1

FIGURE 4

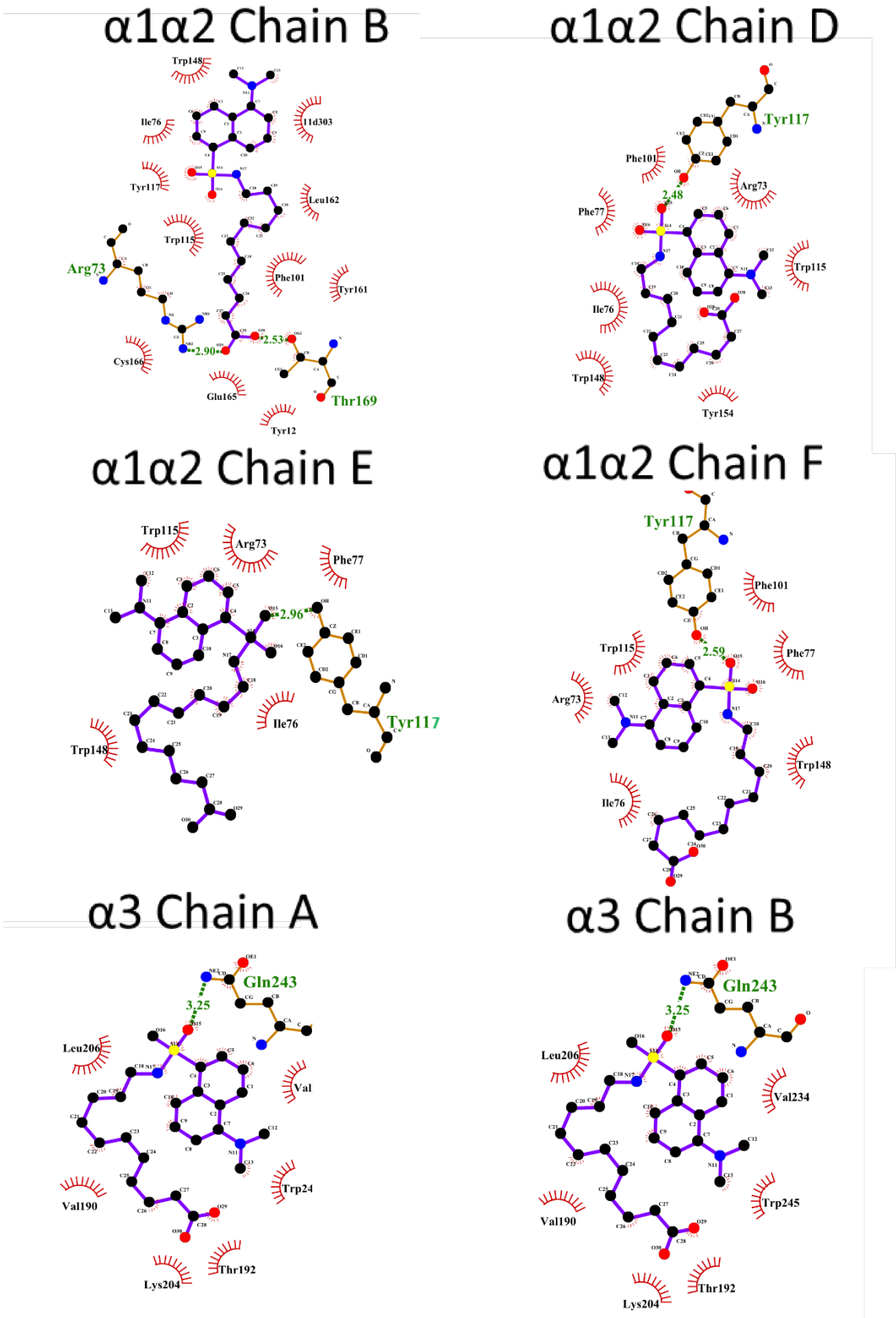
α1α2 Chain B
Trp148
Ile76
11d303
Tyr117
Leu162
Trp115
Arg73
Phe101
Tyr161
2.90
2.53
Cys166
Glu165
Thr169
Tyr12
α1α2 Chain D
Tyr117
Phe101
2.48
Arg73
Phe77
Trp115
Ile76
Trp148
Tyr154
α1α2 Chain E
Trp115
Arg73
Phe77
2.96
Ile76
Tyr117
Trp148
α1α2 Chain F
Tyr117
Phe101
Trp115
2.59
Phe77
Arg73
Trp148
Ile76
α3 Chain A
Gln243
3.25
Leu206
Val
Trp24
Val190
Thr192
Lys204
α3 Chain B
Gln243
3.25
Leu206
Val234
Trp245
Val190
Thr192
Lys204

FIGURE 5

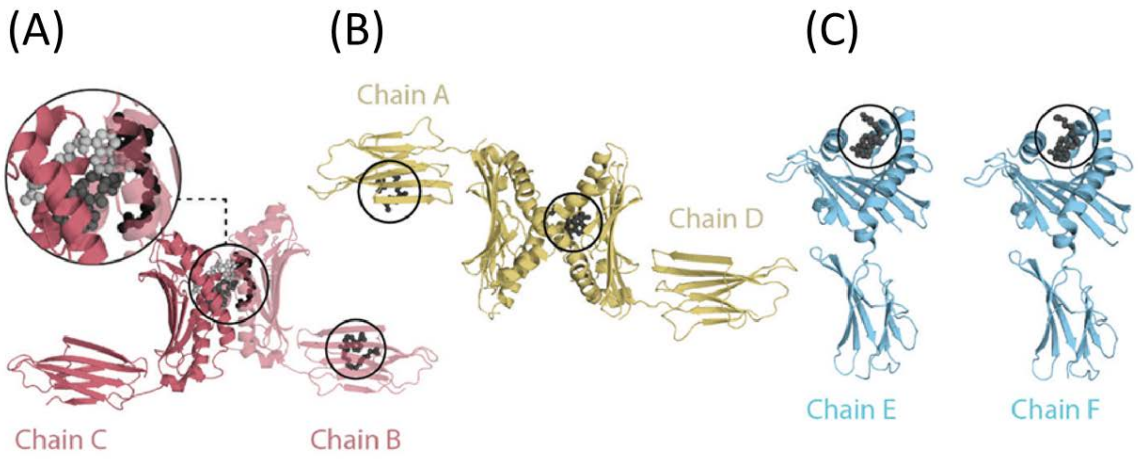

FIGURE 6

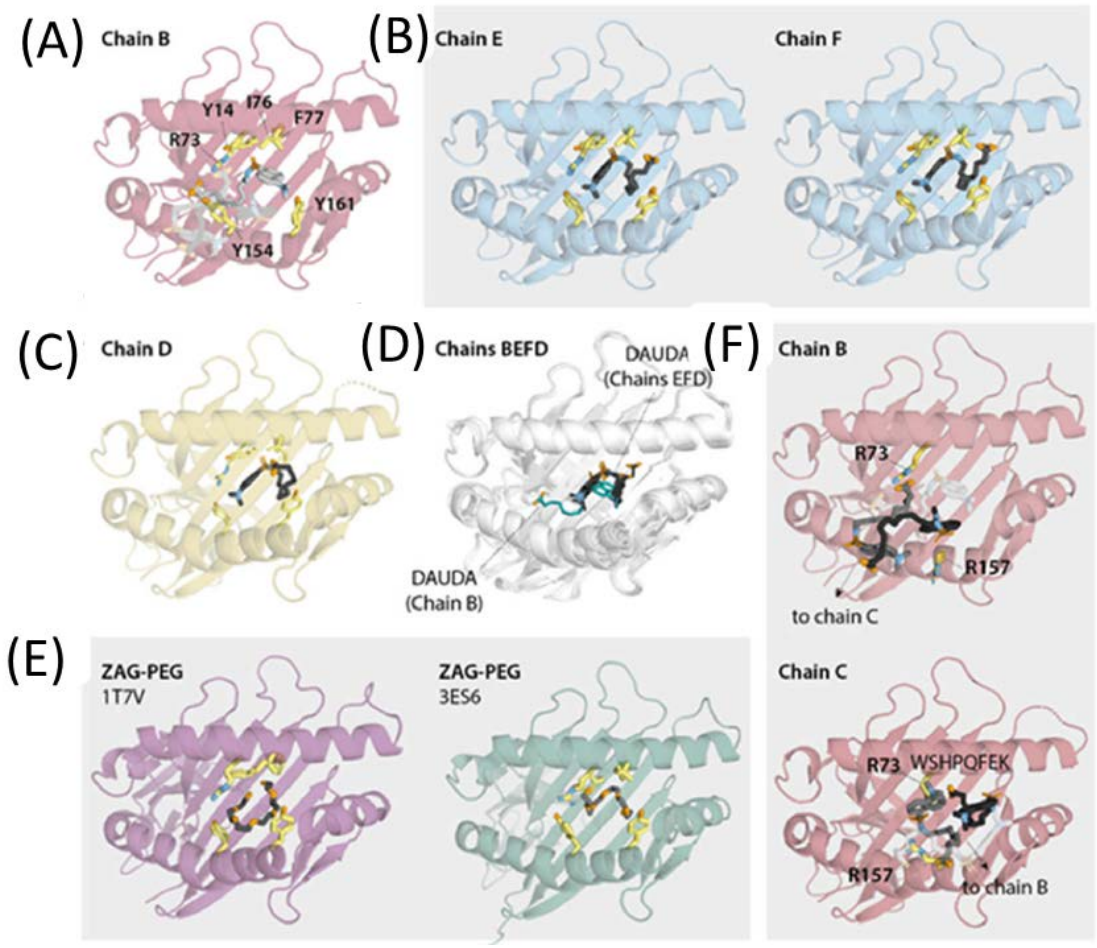
(A)
Chain B
Y14
I76
F77
R73
Y161
Y154
(B)
Chain E
Chain F
(C)
Chain D
(D)
Chains BEFD
DAUDA
(Chains EFD)
DAUDA
(Chain B)
(F)
Chain B
R73
R157
to chain C
(E)
ZAG-PEG
1T7V
ZAG-PEG
3ES6
Chain C
R73
WSHPQFEK
R157
to chain B

FIGURE 7

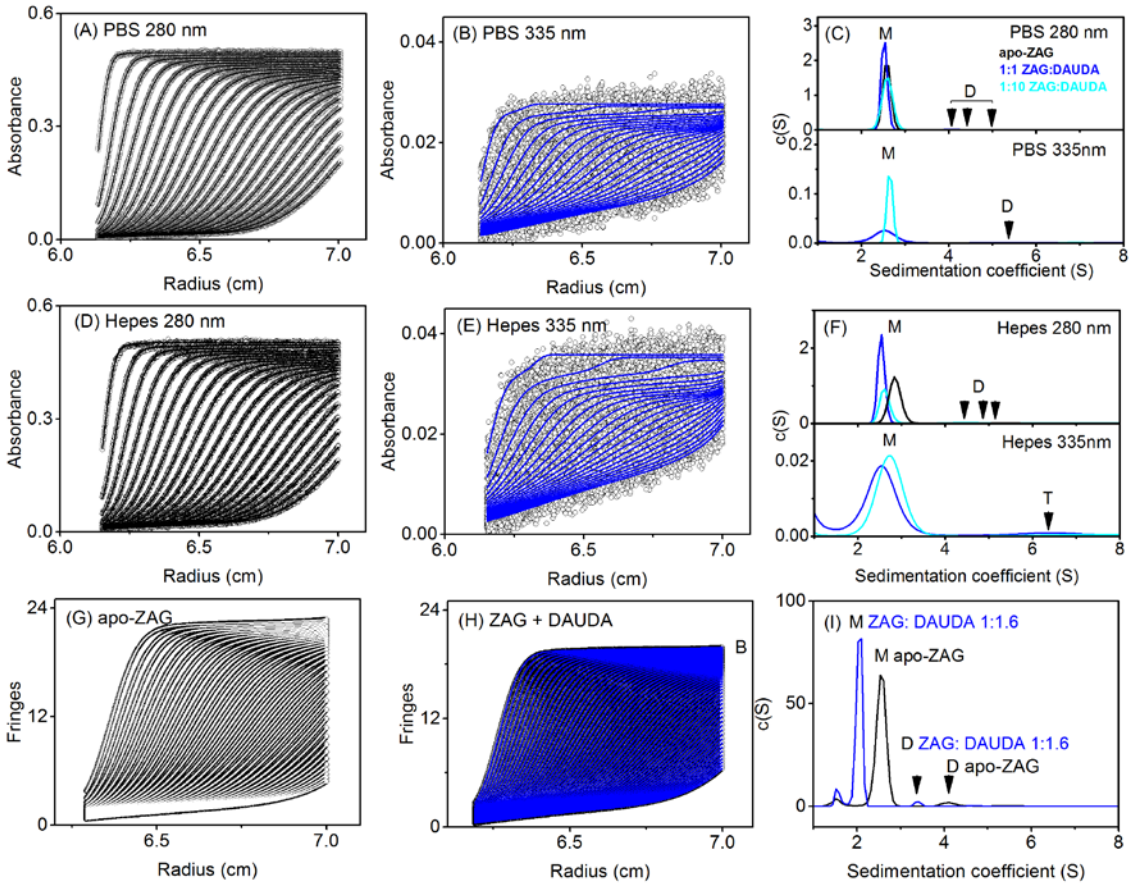
(A) PBS 280 nm
Absorbance
Radius (cm)
(B) PBS 335 nm
Absorbance
Radius (cm)
(C)
M
D
PBS 280 nm
apo-ZAG
1:1 ZAG:DAUDA
1:10 ZAG:DAUDA
c(S)
M
D
PBS 335nm
Sedimentation coefficient (S)
(D) Hepes 280 nm
Absorbance
Radius (cm)
(E) Hepes 335 nm
Absorbance
Radius (cm)
(F)
M
D
Hepes 280 nm
c(S)
M
T
Hepes 335nm
Sedimentation coefficient (S)
(G) apo-ZAG
Fringes
Radius (cm)
(H) ZAG + DAUDA
B
Fringes
Radius (cm)
(I) M ZAG: DAUDA 1:1.6
M apo-ZAG
D ZAG: DAUDA 1:1.6
D apo-ZAG
c(S)
Sedimentation coefficient (S)

FIGURE 8

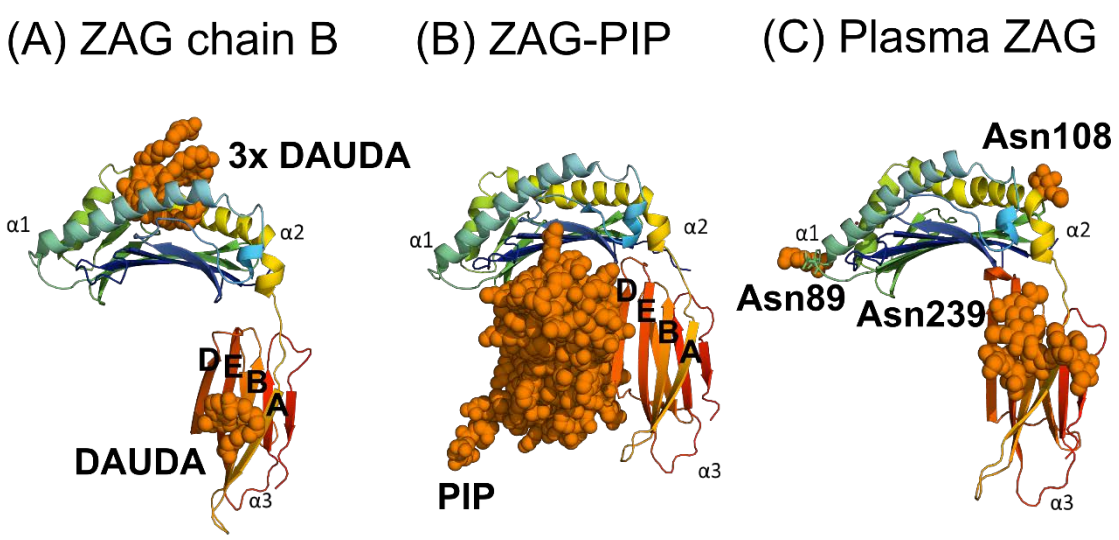
(A) ZAG chain B
(B) ZAG-PIP
(C) Plasma ZAG
3x DAUDA
α1
α2
D
E
B
A
DAUDA
α3
α1
α2
D
E
B
A
α3
PIP
Asn108
α1
α2
Asn89
Asn239
α3

FIGURE 9